A Practical Technique Using Planar Coils to Make the Radiated Immunity of Specific Integrated Circuit Pins Less Dependent From PCB Orientation

Mohsen Koohestani, Mohamed Ramdani, Richard Perdriau

A Practical Technique Using Planar Coils to Make the Radiated Immunity of Specific Integrated Circuit Pins Less Dependent From PCB Orientation

Mohsen Koohestani, *Senior Member, IEEE*, Mohamed Ramdani, *Senior Member, IEEE*, and Richard Perdriau, *Senior Member, IEEE*

***Abstract*—In this article, an inexpensive passive approach is proposed, both making the immunity of integrated circuits (ICs) less dependent on their orientation and controlling the immunity of specific pins. This technique is based on the introduction of planar 2-D coils surrounding the microcontroller (μC) at the printed circuit board (PCB) level. The importance of the coil physical parameters (geometry, resonant frequency, and orientation) as well as the interference frequency is investigated, evaluating the difference in the magnetic field at the pin of interest in two opposite orientations (i.e., 0° and 180°). The effectiveness of the proposed technique is demonstrated in full-wave simulations and measurements, showcasing the provided immunity improvement through monitoring the behavior of the sensitive pins. Besides, this article strongly recommends IC designers not to place power supply pins close to the corners of the μC package due to the presence of the highest local tangential magnetic field when no structures are implemented. Coil orientation is shown to be the key adjustment parameter to enhance the immunity of any specific pin. The resonant frequency of the coils is found to be less relevant than its geometry and distance with respect to the μC pins. The proposed technique using the octagonal coils was also found to be effective in a wide frequency range (from 210 to at least 500 MHz). Compared to a no-coil case, an immunity enhancement of 74.2% (27.5%) is achieved in measurement (simulation) by the addition of an octagonal coil to the PCB, which clearly demonstrates the relevance of that simple approach for practical use in highly sensitive integrated electronics.**

***Index Terms*—Integrated circuit (IC), magnetic field, planar coil, printed circuit board (PCB), radiated immunity.**

I. Introduction

THE accelerated pace of innovation and the industrial electromagnetic compatibility (EMC) trend uphold the enormous demand for the miniaturization of integrated circuits (ICs) with continuously increased functionality at the expense of higher power consumption and switching currents [1]. Such efforts to design a modern microcontroller (μC), which governs specific operations in embedded systems, not only make the μC more prone to a partial or a complete malfunction in the presence of electromagnetic (EM) disturbance but also make it much more challenging to maintain acceptable EMC characteristics. This has led to increasing EMC concerns calling for mitigation techniques to lower emission and susceptibility of printed circuit boards (PCBs) [2].

The first concern in designing a high-speed IC is to properly decouple the power supply pins to keep off conducted fluctuations leading to unwanted radiation and susceptibility [2]. Manufacturers mainly consider the use of metallic or flexible polymer resin, when possible, around the sensitive parts of their products as an EMC shielding technique [3]. The utilization of nonconductive materials is, however, frequently preferred due to being directly applied to IC pins and circuit tracks. In [4], a passive approach using dielectric loading has been proposed to improve the radiated immunity on PCBs independently of frequency with no side effects on the IC performance. In [5], the use of artificially engineered metasurfaces has been investigated to control the frequency of EM waves depending on its geometry and arrangement of the unit structure. A reduced-size frequency selective surface (FSS) has been employed in that study to selectively shield pocket-sized electronic devices against EM disturbances. In [6], an inexpensive shielding technique has been suggested by means of placing a suspended metal loop in proximity to the PCB (as is the case with FSS) to lessen both far-field emission and susceptibility. A methodology, based on small loop theory together with the existence of generated artificial sources due to mirrored image loops, has been provided in that study to analytically predict and further approximate the EM field distribution and strength of an emitting PCB in a couple of seconds, even at very large distances.

The EMC characterization of ICs is of utmost importance to prevent interference issues. Nowadays, the use of full-wave simulations for most of EMC problems is almost inevitable to help EMC engineers better understand the impact of EM disturbances on IC performance [6], [7]. There exist several international EMC guidelines and standards (e.g., IEC and IEEE) specifying essential requirements for electronic products. The radiated immunity of μCs is usually evaluated using direct power injection of EM disturbances to either input or power supply

Manuscript received 24 January 2023; revised 22 March 2023; accepted 27 April 2023. *(Corresponding author: Mohsen Koohestani.)*

The authors are with the ESEO School of Engineering, 49107 Angers, France, and also with the Institute of Electronics and Telecommunications of Rennes, University of Rennes 1, 35042 Rennes, France (e-mail: mohsen.koohestani@eseo.fr; mohamed.ramdani@eseo.fr; richard.perdriau@eseo.fr).

Color versions of one or more figures in this article are available at https://doi.org/10.1109/TEMC.2023.3272020.

Digital Object Identifier 10.1109/TEMC.2023.3272020

pins, following the standards guidelines such as IEC 61967-2 [8]. Depending on the μCs' internal architecture and pin couplings, the susceptibility profile is determined based on the minimum power level required to cause a malfunction and/or degradation of performance.

Transverse electromagnetic (TEM) cells, as far-field free-space condition emulators, have been broadly employed for EMC emission/immunity testing of active components [9], [10]. Below the cutoff frequency of the TEM cell, the latter is assumed to provide a homogeneous EM field distribution with the wave impedance of approximately $120\pi\ \Omega$ ($\approx$377 Ω) within the acceptable working region defined in the IEC 61000-4-20 standard [11]. However, a recent study demonstrated that such cells are not capable of generating uniform fields of known level for accurate and repeatable susceptibility measurements [12]. Nevertheless, such a tool has been widely used to reliably assess emission/immunity levels taking into account the maximum 6-dB variation commonly considered for the primary electrical and magnetic field components [13].

The main goal of this article is, hence, to propose a potential alternative technique to control the distribution of magnetic (H) fields on PCBs, providing an additional degree of freedom not only to make any chosen sensitive pin less susceptible but also to make the IC immunity less dependent from its orientation, depending on the final system-level constraints. Since coils are known to disturb the resulting H-field due to their own generated fields [14], [15], the proposed approach takes benefit of 2-D planar coils of different lengths and geometries surrounding the IC at the PCB level, which properties are assessed through monitoring the behavior of the sensitive pins. Full-wave simulations and measurements are conducted to explore the context and analyze the results.

The rest of this article is organized as follows. Section II describes the simulation and measurement setup configurations. Section III addresses the detailed analysis of the numerical results, while Section IV deals with the experimental results. Finally, Section V concludes this article.

II. Materials and Methods

This section describes the simulation and measurement setups to support the concept of the study investigating the use of planar coils to control $|H|$-fields around an IC mounted on a PCB. All the full-wave simulations are performed using Ansys HFSS computer-aided engineering software [16], with curvilinear meshing applied to all the curved surfaces and volumes (e.g., IC pins and elliptical probing areas) for enhanced accuracy. An average of 2-h simulation time is required with a server having a 20-core CPU running at 2.2 GHz, 512 GB of RAM, and 64 bit Linux.

A. Simulation Setup and Method

In order to present a realistic case study, a 10 cm $\times$ 10 cm four-layer PCB, compliant with IEC 62132-2 [17], is considered. The first and third layers [separated by 0.8-mm-thick FR4 substrate; see Fig. 1(a)] are ground planes, while the second and fourth layers are signal layers. For the sake of simplification, the latter

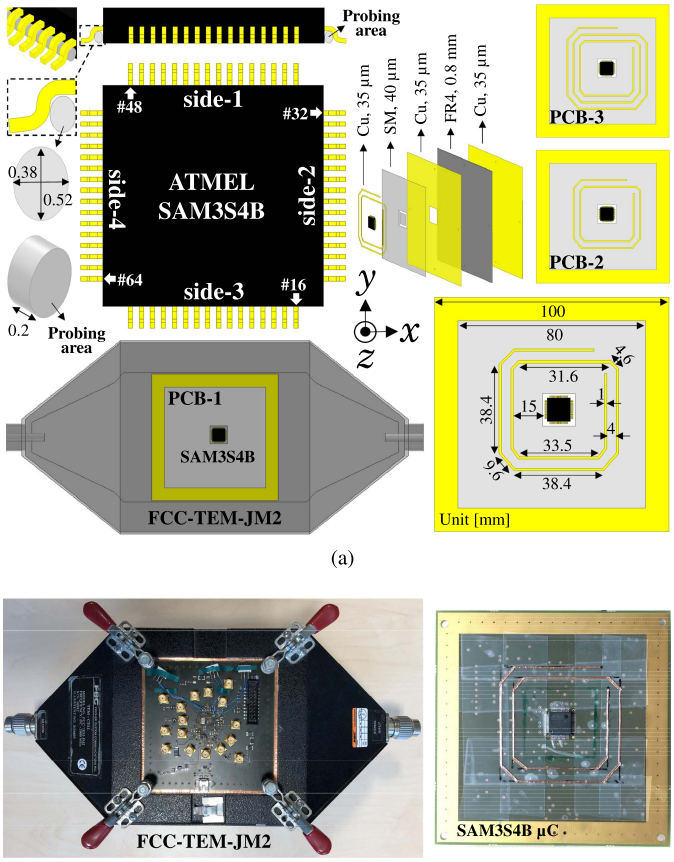

Fig. 1. Test setups for the considered μC placed on a PCB inside the TEM cell. (a) PCB layouts and full-wave simulation setup. (b) Measurement setup.

are not considered in this study, since there are only few conductive copper traces. All the PCB copper planes (represented in yellow) are 35 μm thick.

A 1 cm $\times$ 1 cm 64-pin low-profile quad flat package, representing the ATMEL SAM3S4B μC [18] used for measurements, is placed on the first layer at the same location as on the actual PCB without any ground plane underneath [reproducing the actual PCB; see Fig. 1(a)]. Note that the HFSS 3-D model of the package includes the realistic geometry and dimensions of the package pins; the pins are 0.2 mm wide and separated by 0.3 mm. The four IC sides are considered in the study.

The first layer is coated by a 40-μm-thick soldermask (SM) with $\varepsilon_r = 3.4$ and $\tan\delta = 0.025$ except, of course, under the package pins [see Fig. 1(a)]. Three different PCBs, named PCB-1–PCB-3, are considered in the first part of the study [see Fig. 1(a)]:

1) PCB-1: standard PCB with only the IC;
2) PCB-2 and PCB-3: PCB-1 with added 2-D planar octagonal coils of different lengths (356 and 551 mm for PCB-2 and PCB-3, respectively) with 45° corners for the ease of manufacturing, located 15 mm away from the IC [details can be found in Fig. 1(a)].

Six additional PCBs, including planar spiral coils as well as closed circular and square loops of different radii, will be

studied in Section III-C not only to investigate the importance of geometry (shape and orientation) but also to understand the impact of frequency on magnetic field distribution near the IC.

All the PCBs are placed one by one in an FCC-TEM-JM2 TEM closed cell [19] modeled in HFSS. In order to fairly assess the magnetic field coupling to the package pins, the $|H|$ magnitude is averaged over 3-D ellipses with a thickness identical to the width of the μC pin positioned within the air-filled area below all the pins and PCB [the so-called probing area in Fig. 1(a)]. 1-W power is injected into one port of the septum (the other being terminated with 50 Ω) at 223-MHz frequency, corresponding to the immunity weakness previously observed in measurements [4]. Since the aforementioned weakness was identified to be due to the VDDPLL pin of the μC (pin #64 located in one corner), all the orientations of the PCB are considered in the simulation, which is equivalent to monitoring the four pins indicated by an arrow in Fig. 1(a). The difference in the $|H|$-field obtained at the pin of interest in two opposite orientations along side-2 and side-4 (i.e., 0° and 180°) is considered the metric for that monitoring. Note that additional simulations were carried out to estimate the influence of pin impedance on $|H|$-field distribution. To that end, the previously measured impedance of an SAM3S4B μC power supply pin (extracted from S_{11} measurements and fitted to be equivalent to 5.8 Ω, 12.5 nH, and 510 pF in series in the frequency band of interest) was added between the base of IC corner pins and the ground plane. A difference lower than 1% was observed in the field magnitude compared to the open-circuit pins; hence, this impedance was not considered in the final model.

B. Measurement Setup and Method

After considering several techniques (e.g., thermosensitive materials, embedded loops inside the substrate), it was concluded that there was no practical solution to directly measure the magnetic field at the PCB level near the IC pins without disturbing the field itself. An indirect approach is instead considered to showcase the ability of the proposed technique to control the immunity of the internal phase-locked loop (PLL) of the μC using the same setup as the one described in [4] and modeled in the previous subsection. One of the coils (corresponding to PCB-2) is manufactured from adhesive copper tape and glued to the PCB [see Fig. 1(b)]. Isolating adhesive tape is inserted below in order to avoid short-circuiting existing vias.

The power injection system used in measurement includes a Keysight N5183A RF generator feeding a Prâna AP32DT120 20-W power amplifier. Like in simulations, the amplified RF signal is injected into one port of the TEM cell septum. An 18.432-MHz crystal oscillator feeds the internal PLL of the μC running at 48 MHz. Simple software then toggles an output pin at 1.5 kHz. Like in [4], the immunity criterion is the jitter of the internal PLL, which can be determined by mask testing on the output waveform of the output pin thanks to a Keysight DSO6014L oscilloscope. A square wave is produced by a software-driven output pin. Knowing that the CPU is driven by the PLL output, a PLL failure causes a frequency deviation or phase deviation (jitter) in that waveform. A mask is defined around the nominal waveform with a small deviation (5%) in the time domain. A failure is triggered as soon as the acquired waveform overshoots that mask. A task is equivalent to a self-timed automatic comparison between the waveform and the mask; hence, the failure rate is the ratio of the number of failures divided by the number of tasks. The test is carried out in a 1-min time slot. The criterion for insensitivity to orientation is the ratio of the number of failures in one given orientation of the PCB divided by the number of failures in the opposite orientation (i.e., 0° and 180°).

III. Simulation Results and Discussion

This section addresses the simulation results to showcase the importance of the introduced 2-D coils around the μC. The $|H|$-field strength averaged over the elliptical probing areas is monitored in the presence and absence of the coils.

A. Coil Resonant Frequency

With the aim to demonstrate the role of the coil resonant frequency in our study, a modal analysis based on the theory of characteristic modes was first carried out in HFSS in free space. It was found that the shorter and longer coils are strongly resonant, with an unity modal significance and a 180° characteristic angle [20] at 350 and 206 MHz, respectively.

In the presence of the PCB, owing to the need for huge computational power, modal analysis is usually performed either without the dielectric material and ground plane or with lossless substrates and zero thickness perfect electric conductors (see, e.g., [20] and [21]) at the expense of affecting the accuracy of the modal resonances, even if a frequency downshift should still be expected. Unfortunately, the latter simulation in free space is the only that could be implemented by the authors. However, in order to obtain a very close estimation of the coils' resonant frequencies in their actual environment (PCB-2 and PCB-3), the formulations provided in [22] were used. According to the latter, the approximated resonant frequencies of the shorter and longer coils, only taking into account the electrical properties of the SM and the first ground plane, were found to be 230 and 150 MHz, respectively.

B. Coil Influence on Magnetic Field

In order to understand the impact of the planar coils, a comparison was made in the presence (PCB-2 and PCB-3) and absence (PCB-1) of the designed coils. Fig. 2 exhibits the distribution of the $|H|$-field magnitude averaged over the elliptical probing areas along the four sides of the chip at 233 MHz, whereas Fig. 3 displays the $|H|$-field difference (in mA·m^{-1}) between the pins in the opposite (0° and 180°) sides.

In order to properly analyze the obtained results, the magnitude and orientation of the tangential H-field with respect to the μC pins at the frequency of interest have to be first verified to indicate whether or not the fields couple to the pins of interest. For that purpose, the distribution of the vector H-field at the ellipse-center level was simulated for PCB-1–PCB-3 (see Fig. 4). As observed, the privileged orientation of the fields is parallel to the y-axis, being parallel to μC package pins in side-1

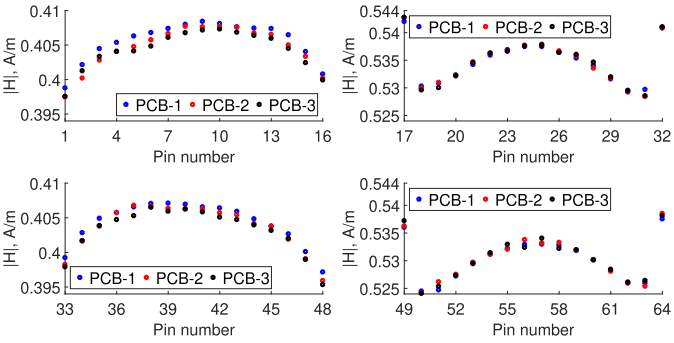

Fig. 2. $|H|$-field magnitude averaged over the elliptical probing areas for 1-W input power at 233 MHz for PCB-1–PCB-3.

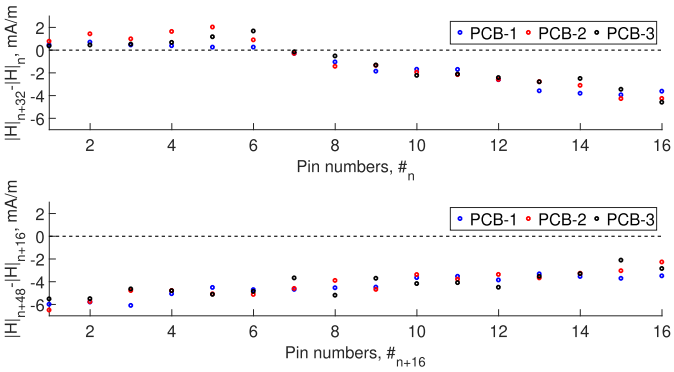

Fig. 3. $|H|$-field difference between the pins in opposite sides for the results in Fig. 2: (top) side-1 and side-3 and (bottom) side-2 and side-4.

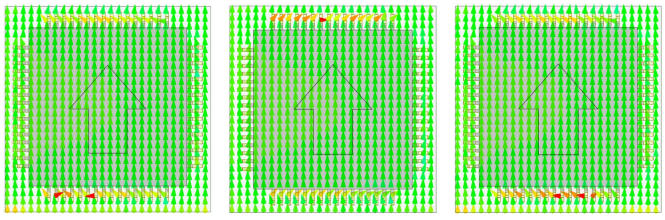

Fig. 4. Vector H-field distribution at the ellipse-center level for 1-W input power at 233 MHz in (a) PCB-1, (b) PCB-2, and (c) PCB-3. Scale: logarithmic with 15 subdivisions ranging from $1E^{-1}$ to $8E^{-1}$ A· m^{-1}. Black arrow indicates the privileged orientation.

and side-3. That confirms that almost no coupling to the μC pins occurs at those sides of the IC; therefore, no further analysis is provided in the rest of this article. Conversely, the direction of the field at locations where the field lines are parallel to side-2 and side-4 and, consequently, perpendicular to μC package pins, leads to maximum field coupling to the pins. The higher field-to-pin coupling explains the different results in side-2 and side-4 compared to side-1 and side-3 (see Fig. 2). Note that the high-intensity spots at different locations near the pins along side-1 and side-3 were verified not to be perpendicular to the pins; the very similar magnitude of the $|H|$-field in the studied cases near those package sides is evident in Fig. 2.

A first look at the results obtained at the pin locations in two opposite orientations along side-2 and side-4 (i.e., 0° and

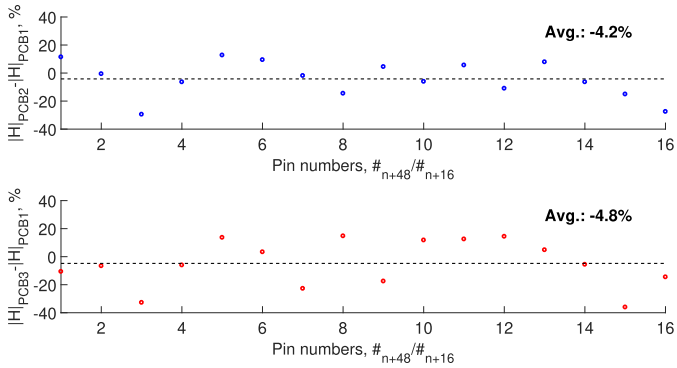

Fig. 5. $|H|$-field difference (in %) between PCB-2 (top) and PCB-3 (bottom) from PCB-1 for pins along side-2 and side-4. Input power: 1 W at 233 MHz. The black dashed lines indicate the average value over the considered sides.

180°) shows that, no matter if the coils are present or not, the difference in the averaged field strength between corner pins and their adjacent pins is approximately 5.2 times (∼+423%, #30/#29 = 0.47% compared with #32/#31 = 2.46%) as high as the highest difference between other neighboring pin pairs (see Fig. 2). That was observed in all the different scenarios considered in the study. This provides a sensible guideline for IC designers not to place low-impedance pins (such as power supplies) at the extreme corner of the chip due to the presence of the highest local tangential $|H|$-field. Moreover, a higher field level in side-2 rather than side-4 can be noticed resulting in a negative percentage difference between the corresponding pins in those opposite sides (see Fig. 3, bottom). Such a phenomenon can only be demonstrated by full-wave simulation as the wave impedance near the IC differs from that inside the TEM cell (i.e., 377 Ω) and varies along each of the package sides. That highlights the dependence of the immunity of ICs on their orientation, specifically in a real-world system where the PCB can be placed with any orientation with respect to the existing EM interference.

In order to evaluate the extent of the change in $|H|$-field intensity brought by the introduction of the coils around the μC, Fig. 5 plots the $|H|$-field difference (in %) between PCB-2 and PCB-3 from PCB-1 for the pins along side-2 and side-4. As can be seen, the addition of the shorter and longer coils leads to a lower $|H|$-field intensity at the location of pin of interest (#64/#32) by 27.5% and 14.5%, respectively, in comparison to the no-coil case (PCB-1). This implies that a lower difference in the immunity of the VDDPLL pin of the μC between both the PCB orientations should be expected in measurements. Moreover, the averaged difference between opposite pins is lower by 4.2% and 4.8% compared to PCB-1 for PCB-2 and PCB-3, respectively, which demonstrates a lower sensitivity to orientation in PCB-2 and PCB-3 compared to PCB-1. It can be noted that the similarity in that averaged difference, whatever the coil (see Fig. 5), indicates that the resonant frequency of the coil may not play an important role in making the pins less sensitive (in average) to orientation. However, some opposite pin pairs may exhibit higher field difference on PCB-2 and PCB-3 compared to PCB-1 depending on their location. This must be

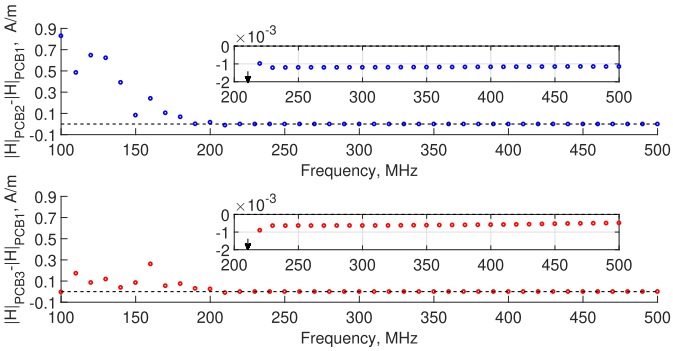

Fig. 6. $|H|$-field difference between the pins of interest (#64/#32) as a function of frequency for 1-W input power; PCB-2 (top) and PCB-3 (bottom) compared to PCB-1.

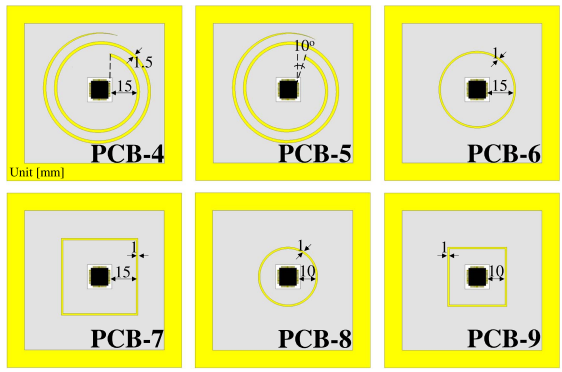

Fig. 7. Layout of the studied PCBs to assess the importance of coil geometry.

taken into account when applying this method to μCs for which power supply pins are not located in the corners.

C. Importance of Frequency

With the aim to investigate the suitability of the technique in case of broadband interference, a further study was conducted to assess the frequency range where the coils are capable of providing less sensitivity to PCB orientation. For that purpose, the frequency was swept from 100 to 500 MHz with 10-MHz steps, and the differences among the studied PCBs at the pin of interest in side-2 and side-4 (i.e., #64/#32) were evaluated; results are shown in Fig. 6.

Within the monitored frequency range, for both the coils (PCB-2 and PCB-3), the expected behavior is attainable at frequencies above 210 MHz (see Fig. 6). Moreover, in that range, the average improvement provided by the shorter coil is around 48% better than for the longer coil. These results clearly showcase the effectiveness of the planar coils to adjust the $|H|$-field distribution near the sensitive pin of the chip in a wide frequency range.

D. Importance of Coil Geometry

Since the amount of induced current on the coils and, consequently, self-produced fields (Faraday's law) depends on the coil geometry, the importance of the latter was investigated by modifying the coil shape, size, and orientation. Fig. 7 shows the layout of the studied PCBs. For a fair comparison, a minimum of 15-mm gap was kept between the added structures to PCB-1 and the μC pins. The $|H|$-field difference (in %) between each of the PCBs and PCB-1 for the pins along side-2 and side-4 is plotted in Fig. 8 for an input power of 1 W at 233 MHz. Note that, for all the considered PCBs, the orientation of the vector H-field distribution was verified in simulations to be along the y-axis; therefore, results obtained for side-1 and side-3 were ignored.

1) Spiral Coil: As a showcase, an Archimedean spiral with an inner radius of 20 mm, two turns, and one arm was first added to PCB-1 at the same location where the octagonal coils were previously placed (forming PCB-4; see Fig. 7). As

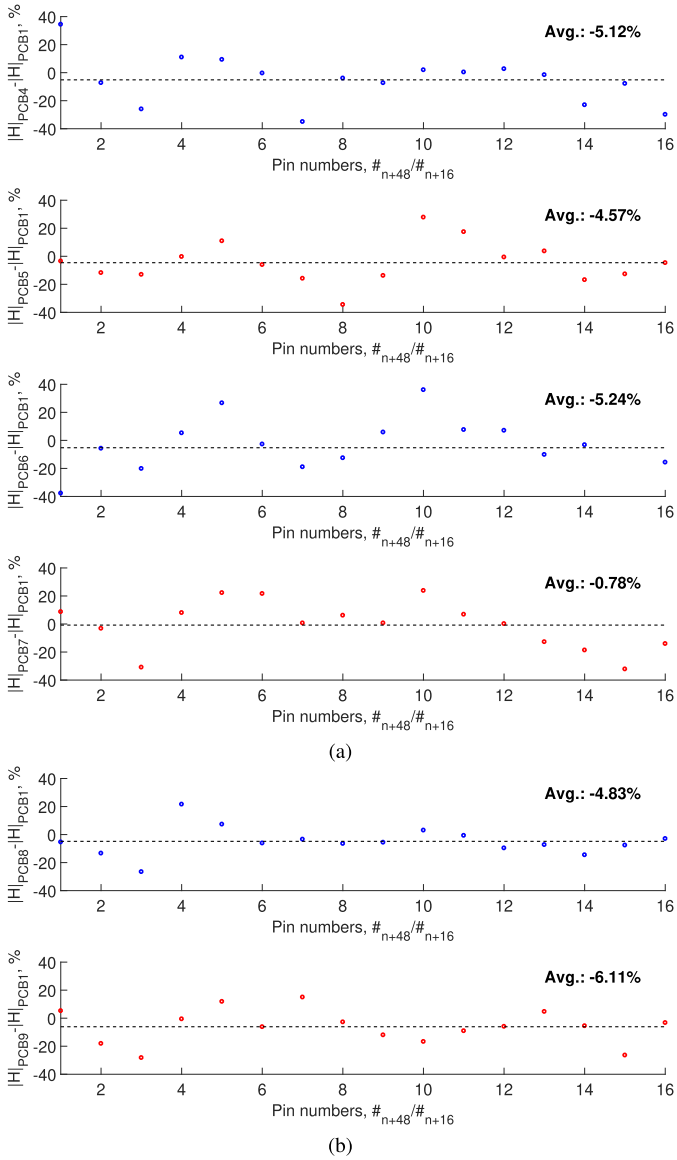

Fig. 8. $|H|$-field as a function of coil geometry for 1-W input power at 233 MHz: difference (in %) between (a) PCB-4 and PCB-7, and (b) PCB-8 and PCB-9, from PCB-1 across the pins along side-2 and side-4. The black dashed lines indicate the average value over the considered sides.

TABLE I
AVERAGED $|H|$ DIFFERENCE BETWEEN OPPOSITE PINS OF SIDE-4 COMPARED WITH SIDE-2 FOR ALL THE CONSIDERED PCBS

DUT	Average ($\|H\|$)
PCB-1	–4.44 mA·m^{-1}
PCB-2	–4.25 mA·m^{-1}
PCB-3	–4.23 mA·m^{-1}
PCB-4	–4.22 mA·m^{-1}
PCB-5	–4.24 mA·m^{-1}
PCB-6	–4.21 mA·m^{-1}
PCB-7	–4.41 mA·m^{-1}
PCB-8	–4.23 mA·m^{-1}
PCB-9	–4.17 mA·m^{-1}

observed, such a coil not only provides a slightly lower (by 2.3 percentage point [pp]) $|H|$-field difference between pins of interest (#64/#32) compared to the octagonal one but also leads to a 0.9 pp enhancement in the overall averaged difference [Fig. 8(a), top, compared with Fig. 5, top]. The latter is less pronounced (0.3 pp) compared with that achieved by the longer octagonal coils [Fig. 8(a), top, compared with Fig. 5, bottom].

It is important to note that although the coil resonant frequency does not play a major role, full-wave simulation is still required to find the appropriate orientation of the coil depending on the μCs' package size, coil-to-pin distance, and location of the target pin. To showcase the importance of the coil orientation, the spiral coil in PCB-4 was rotated clockwise by only 10° around the z-axis (PCB-5 in Fig. 7). As can be visually seen in Fig. 8(a), that tiny rotation leads to a 0.55 pp deterioration in the $|H|$-field averaged difference compared to PCB-4. Moreover, at the pins of interest, the $|H|$-field difference is increased by 25 pp for PCB-4 compared with PCB-5: the effect of the rotated coil is much less pronounced for those pins. Therefore, changing the orientation of the coil can be considered a solution for cases where the location of the sensitive pin is different (and not necessarily in the package extreme corners).

2) Circular/Square Loop: A further study was also conducted to investigate the suitability of the proposed approach in the case of employing closed circular (PCB-6) and square (PCB-7) loops (see Fig. 7). As observed in Fig. 8, whatever the loop geometry, the decrease in sensitivity to orientation is evident when compared the no-coil case. In spite of having simpler structure, at the location of the pins of interest, the $|H|$-field difference in the presence of both the loops is raised compared to the cases with the octagonal or spiral coils, e.g., increased by 12.4 pp and 14 pp when comparing PCB-6 and PCB-7 to PCB-2, respectively [Fig. 8(a) compared with Fig. 5].

Unlike in coils where rotation can be a degree of freedom, the use of such loops may not be very effective in cases where the location of the sensitive pin is different. Simulations were, however, repeated with different loop radii, considering a 10-mm (instead of 15-mm) loop-to-pin distance, to further showcase the influence of the loop size. As can be seen in Fig. 8(b), although a higher $|H|$-field difference at the location of the target pins was obtained (by 13.4 pp and 10.9 pp when comparing PCB-6 and PCB-7 to PCB-8 and PCB-9, respectively), a higher (by

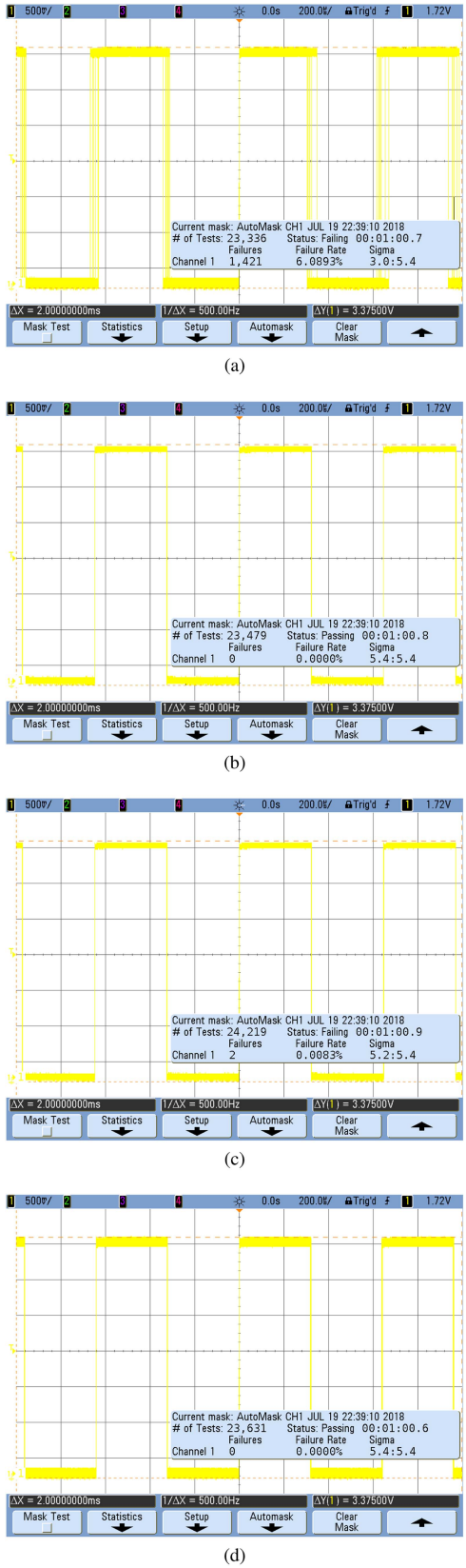

Fig. 9. Measured μC failure rate for PCB-1 averaged over a 1-min time slot for a 20-W input power at 223 MHz and four different orientations. (a) 0°, (b) 90°, (c) 180°, and (d) 270°.

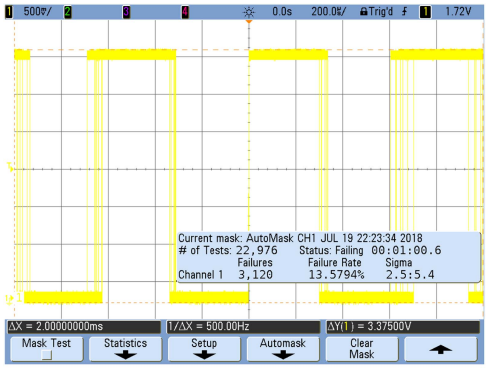

(a)

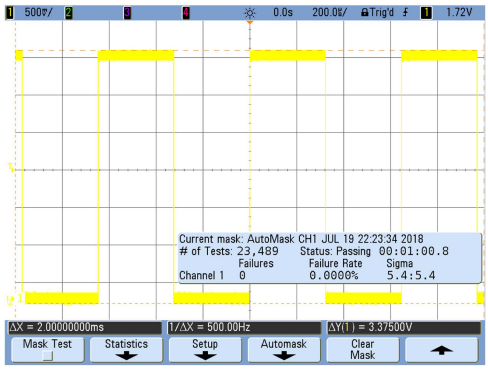

(b)

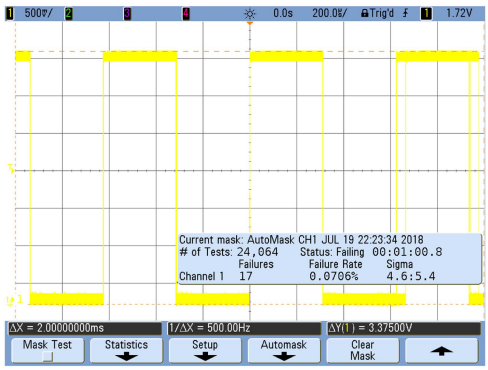

(c)

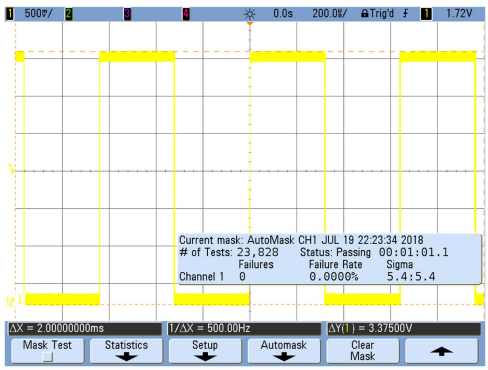

(d)

Fig. 10. Measured μC failure rate for PCB-2 averaged over a 1-min time slot for a 20-W input power at 223 MHz and four different orientations. (a) 0°, (b) 90°, (c) 180°, and (d) 270°.

5.3 *pp*) averaged insensitivity improvement was achieved with the square loop [Fig. 8(a) compared with Fig. 8(b)]. Therefore, the use of closed loops can also be of interest to some extent when properly designed.

To sum up, whatever the coil geometry, a reduction in the overall averaged differences was achieved, as can be seen in Table I. Depending on the dimensions and arrangement of the μC pins, a simple closed loop with any geometry, which is indeed more practical to fabricate compared to planar coils, can be considered, but no degree of freedom is available with respect to coils in cases where the location of the sensitive pin is not exactly in one corner of the chip. Moreover, the coil orientation and distance to IC pins have to be optimally chosen, which requires full-wave analysis.

IV. Measurement Results and Discussion

In order to validate the proposed technique, even though the spiral coil was found to provide a lower $|H|$-field difference at the pin of interest (#64/#32) compared to the octagonal one, the latter with the shorter length was implemented for the ease of fabrication [see Fig. 1(b)]. Note that although a lower averaged difference at pins along side-2 and side-4 was achieved with the spiral coil as well as with the circular and square loops compared with the octagonal coil, those structures were not chosen due to a higher field difference at the target pin depending on orientation. PCB-1 and PCB-2 were successively illuminated in the TEM cell with 20 W at 223 MHz. For each PCB, the four possible orientations were tested, with the PLL jitter (propagated to the output pin jitter) as the immunity criterion. Measured results are displayed in Figs. 9 and 10 for PCB-1 and PCB-2, respectively, with the experimental data summarized in Table II. Each figure indicates the number of failures over a 1-min time slot.

As can be seen, no failures were monitored in the 90° and 270° orientations, on either PCB [see Figs. 9 and 10(b) and (d)]. This result was expected due to the magnetic field being parallel to the IC pins in both the cases [see Fig. 4]. This is also in line with the full-wave simulations (side-1 and side-3).

As far as 0° and 180° orientations were concerned, a significant difference could be observed in failure rates. More specifically, the failure rate ratios between both the orientations were 710.5 and 183.5 for PCB-1 and PCB-2, respectively. This yields to a 74.2% improvement of the failure rate ratio in the presence of the octagonal coil due to a better magnetic field uniformity between both the pin locations. Absolute failure rates were not taken into account, since the objective of the present study is related to the insensitivity to PCB orientation, not to absolute immunity levels. It is also worth mentioning that no failures were observed at other frequencies ranging from 1 MHz to 1 GHz for both the PCBs.

To sum up, the suitability of the proposed technique was demonstrated to significantly decrease the influence of IC orientation on the immunity performance of a highly sensitive μC to a tangential $|H|$-field coupled to its power supply pins, having no adverse effect on its functionality. Measurements were in line

TABLE II
SAM3S4B μC EXPERIMENTAL DATA FOR PCB-1 AND PCB-2 AVERAGED OVER A 1-MIN TIME SLOT AT DIFFERENT ORIENTATIONS

Parameters	PCB-1				PCB-2			
	0°	90°	180°	270°	0°	90°	180°	270°
Num. of tasks	23 336	23 479	24 219	23 631	22 976	23 489	24 064	23 828
Failures	1421	0	2	0	3120	0	17	0
Failure rate	6.1%	0%	0.01%	0%	13.6%	0	0.07%	0%
Sigma	3:5.4	5.4:5.4	5.2:5.4	5.4:5.4	2.5:5.4	5.4:5.4	4.6:5.4	5.4:5.4

with simulations, where the latter was found to very helpful to deeply analyze and more clearly understand the physics behind the studied case. Note that a lower insensitivity improvement near the target pin in simulations (27.5%) compared to that of measurements (74.2%) can be due to the considered probing area, as well as possible couplings to other VDD pins, which were not taken into account in simulations.

V. CONCLUSION

This article not only showcased the importance of the full-wave analysis to better understand the physics behind a known EMC issue of an IC but also provided a reliable solution to that problem. According to the full-wave simulations, at locations where the orientation of the tangential magnetic field was perpendicular to the μC pins (leading to increased coupling), the illumination of corner pins was much higher than others, and seeing that the orientation of the IC with respect to field propagation matters for their immunity, this clearly explained the immunity weakness of the VDDPLL pin (#64 located in one corner) of the studied SAM3S4B μC. Planar 2-D coils surrounding the μC were introduced at the PCB level to make the radiated immunity of the package pin of interest less sensitive to orientation. This was specifically interesting in a real-world system where a PCB may be placed anywhere, with any orientation with respect to the existing EM interference. Therefore, the presented technique can be used to mitigate the susceptibility of an IC placed in a system by reducing the latter's dependence on the distribution of magnetic field and, consequently, the risk of susceptibility.

The importance of the coil physical parameters (geometry, resonant frequency, and orientation) as well as the interference frequency was examined. $|H|$-field strength averaged over the defined probing areas below the μC pins was compared in the presence and absence of the coils. The following observations were made for the considered case study.

1) The highest local tangential magnetic field often occurred close to the corners of the μC package. This can be considered an important guideline for IC designers not to place the power supply pins at the extreme corners of the chip.
2) Whatever the coil geometry, improvement in the overall averaged $|H|$-field difference was achieved.
3) The capability of a representative octagonal coil to provide less sensitivity to PCB orientation was demonstrated in simulations (measurements) in a wide frequency range from 210 (1) MHz to at least 0.5 (1) GHz.
4) Compared to a no-coil case, a reduction of 74.2% (27.5%) of the sensitivity to orientation was obtained in measurement (simulation) by the addition of an octagonal coil to the PCB.
5) The resonant frequency of the coils was found to be less relevant than its geometry and distance with respect to the μC pins, whereas the coil orientation was shown to be the key modifying parameter for cases with the location of the sensitive pin among the middle pins.
6) A simple closed loop of whatever the geometry can also improve the overall averaged $|H|$-field difference between opposite orientations, bearing in mind that it may not be very effective in cases with the sensitive pin among the middle pins of the chip.
7) By rotating the coils, the insensitivity to orientation can be enhanced for other pins as those located in the corners.
8) The suitability of the proposed technique was demonstrated to decrease the influence of IC orientation on the immunity performance of a highly sensitive μC to a tangential $|H|$-field coupled to its power supply pins, having no adverse effect on its functionality.

REFERENCES

[1] S. C. Folea and G. D. Mois, "Lessons learned from the development of wireless environmental sensors," *IEEE Trans. Instrum. Meas.*, vol. 69, no. 6, pp. 3470–3480, Jun. 2020.
[2] S. Ben Dhia, M. Ramdani, and E. Sicard, *Electromagnetic Compatibility of Integrated Circuits: Techniques for Low Emission and Susceptibility*. Berlin, Germany: Springer, 2006.
[3] R. Valente, C. D. Ruijter, D. Vlasveld, S. V. D. Zwaag, and P. Groen, "Setup for EMI shielding effectiveness tests of electrically conductive polymer composites at frequencies up to 3.0 GHz," *IEEE Access*, vol. 5, pp. 16665–16675, 2017.
[4] M. Koohestani, R. Perdriau, J.-L. Levant, and M. Ramdani, "A novel passive cost-effective technique to improve radiated immunity on PCBs," *IEEE Trans. Electromagn. Compat.*, vol. 61, no. 6, pp. 1733–1739, Dec. 2019.
[5] M. Koohestani, R. Perdriau, M. Ramdani, and J. Carlsson, "Frequency selective surfaces for electromagnetic shielding of pocket-sized transceivers," *IEEE Trans. Electromagn. Compat.*, vol. 62, no. 6, pp. 2785–2792, Dec. 2020.
[6] M. Koohestani, A. K. Skrivervik, and M. Ramdani, "An analytical approach for the estimation of the far-field reduction obtained by placing closed conductor loops in proximity to a chip," *IEEE Trans. Electromagn. Compat.*, vol. 63, no. 5, pp. 1384–1394, Oct. 2021.
[7] R. Mittra, *Computational Electromagnetics: Recent Advances and Engineering Applications*, 1st ed. New York, NY, USA: Springer, 2013.
[8] Integrated Circuits, Measurement of Electromagnetic Emissions, 150 kHz to 1 GHz, Measurement of Radiated Emissions—TEM Cell and Wideband TEM Cell Method, Standard IEC 61967-2, 2005.
[9] M. L. Crawford and J. L. Workman, "Using a TEM cell for EMC measurements of electronic equipment," U.S. Dept. Commerce, Nat. Bureau Standards, Gaithersburg, MD, USA, 1979.
[10] M. Kanda and R. D. Orr, "Generation of standard electromagnetic fields in a TEM cell," U.S. Dept. Commerce, Nat. Bureau Standards, Gaithersburg, MD, USA, 1988.

[11] Testing and Measurement Techniques—Emission and Immunity Testing in Transverse Electromagnetic (TEM) Waveguides, Standard IEC 61000-4-20, 2010.
[12] M. Koohestani, M. Ramdani, P. Besnier, J.-L. Levant, and R. Perdriau, "Perturbations of electric and magnetic fields due to the presence of materials in TEM cells," *IEEE Trans. Electromagn. Compat.*, vol. 62, no. 4, pp. 997–1006, Aug. 2020.
[13] B. Korber, M. Trebeck, N. Muller, F. Klotz, and V. Mullerwiebus, "IC-strip line—A new proposal for susceptibility and emission testing of ICs," in *Proc. Int. Workshop EMC COMPO*, 2007, pp. 125–129.
[14] Y. Liyuan, L. Shushu, N. Pingjuan, S. Hao, M. Run, and C. Zheng, "Novel square spiral coil for achieving uniform distribution of magnetic field," *IOP Conf. Ser.: Earth Environ. Sci.*, vol. 332, no. 4, 2019, Art. no. 042005.
[15] P. Andris, J. Weis, and I. Frollo, "Magnetic field of spiral-shaped coil," in *Proc. 7th Int. Conf. Meas.*, 2009, pp. 262–265.
[16] *Ansys Electromagnetic Suite 2021/R2, High Frequency Structure Simulator (HFSS)*, Ansys, Inc., Pittsburgh, PA, USA, 2021.
[17] Integrated Circuits, Measurement of Electromagnetic Emissions, 150 kHz to 1 GHz, Measurement of Radiated Immunity—TEM Cell and Wideband TEM Cell Method, Standard IEC 62132-2, 2010.
[18] "Microchip SAM3S series microcontrollers, ATSAM3S4B." Accessed: Mar. 16, 2023. [Online]. Available: https://www.microchip.com/en-us/product/ATSAM3S4B
[19] Tekbox TBTC1 TEM Cell for EMC Pre-compliance Testing, Rekirsch Elektronik Inc., Vienna, Austria. Accessed: May 5, 2023. [Online]. Available: https://www.rekirsch.at/cgi-bin/lshop.cgi?ls=de&eix=1282834349&action=showdetail&quicksearch=1&ssl=1&artnum=TBTC1
[20] D. Y. Chen and C.-F. Wang, *Characteristic Modes: Theory and Applications in Antenna Engineering*. Hoboken, NJ, USA:Wiley, 2015.
[21] D. Wen, Y. Hao, H. Wang, and H. Zhou, "Design of a wideband antenna with stable omnidirectional radiation pattern using the theory of characteristic modes," *IEEE Trans. Antennas Propag.*, vol. 65, no. 5, pp. 2671–2676, May 2017.
[22] I. J. Bahl, *Lumped Elements for RF and Microwave Circuits*. Norwood, MA, USA: Artech House, 2003.

Mohsen Koohestani (Senior Member, IEEE) received the Ph.D. (Hons.) degree in electromagnetics from the École Polytechnique Fédérale de Lausanne, Lausanne, Switzerland, and the Universidade de Lisboa, Lisbon, Portugal, in 2014.

From 2014 to 2018, he was a Senior Research Fellow with the Institute of Electronics and Telecommunications of Rennes, University of Rennes 1, Rennes, France, working mainly on biomedical applications of wireless power transfer systems. Since 2018, he has been an Associate Professor with the ESEO School of Engineering, Angers, France. He is also an Associate Researcher with the Institute of Electronics and Telecommunications of Rennes, UMR CNRS 6164, Rennes. He has authored more than 70 peer-reviewed scientific papers. His main research interests include antennas, microwaves, electromagnetic compatibility (EMC), and biomedical engineering.

Dr. Koohestani is an Official Member of AFNOR, the IEC standardization working groups (WG2 and WG9) in the SC47A French Subcommittee on the EMC for integrated circuits.

Mohamed Ramdani (Senior Member, IEEE) was born in Oujda, Morocco. He received the Ph.D. degree in microelectronics from Université Paul Sabatier, Toulouse, France, in 1989, and the "Habilitation á Diriger des Recherches" (Accreditation degree) from the Université de Rennes 1, Rennes, France, in 2004.

From 1991 to 2008, he was an Associate Professor of Microelectronics and Microwave Electronics with the ESEO School of Engineering, Angers, France, where he became a Full Professor in 2008. His research interests include electromagnetic compatibility (EMC) of integrated circuits and integrated circuit design. He has authored several book chapters on EMC of integrated circuits and many peer-reviewed scientific papers.

Dr. Ramdani is a Member of AFNOR (French section of the International Electrotechnical Commission). He was the General Chair of 2017 International Symposium on Electromagnetic Compatibility, Angers. He was the Vice-Chair of the IEEE France Section in 2016.

Richard Perdriau (Senior Member, IEEE) was born in Angers, France, in 1971. He received the Engineering degree in electronics and computer science from the ESEO School of Engineering, Angers, in 1992, Ph.D. degree in applied sciences from the Université Catholique de Louvain, Louvain-la-Neuve, Belgium, in 2004, and the "Habilitation á Diriger des Recherches" (Accreditation Degree) from the Université de Rennes 1, Rennes, France, in 2012.

From 1992 to 2012, he was an Associate Professor of Microelectronics and Embedded Systems with the ESEO School of Engineering, where he became a Full Professor in 2013. His research interests include electromagnetic compatibility of integrated circuits, mixed-signal hardware description languages, and integrated circuit design.

Dr. Perdriau was the Vice-Chair and Technical Program Co-Chair of 2017 International Symposium on Electromagnetic Compatibility.